24-mar-1992

Local Particle Densities and Global Multiplicities in Central Heavy Ion Interactions at 3.7, 14.6, 60 and 200 A GeV.

EMU01 - collaboration

M I Adamovich[13], M M Aggarwal[4], Y A Alexandrov[13], N P Andreeva[1], Z V Anson[1], R Arora[4], F A Avetyan[20], S K Badyal[8], E Basova[17], K B Bhalla[7], A Bhasin[8], V S Bhatia[4], V G Bogdanov[15], V I Bubnov[1], T H Burnett[16], X Cai[18], I Y Chasnikov[1], L P Chernova[18], M M Chernyavsky[13], G Z Eligbaeva[1], L E Eremenko[1], A S Gaitinov[1], E R Ganssauge[12], S Garpman[11], S G Gerassimov[13], J Grote[16], K G Gulamov[18], S K Gupta[7], V K Gupta[8], H H Heckman[3], H Huang[19], B Jakobsson[11], B Judek[14], L Just[9], S Kachroo[8], G S Kalyachkina[1], E K Kanygina[1], M Karabova[6,9], G L Kaul[8], S Kitroo[8], S P Kharlamov[13], S A Krasnov[6], S Kulikova[6], V Kumar[7], P Lal[7], V G Larionova[13], V N Lepetan[1], L S Liu[18], S Lokanathan[7], J Lord[16], N S Lukicheva[18], S B Luo[10], T N Maksimkina[6], L K Mangotra[8], N A Marutyan[20], N V Maslennikova[13], I S Mittra[4], S Mookerjee[7], H Nasrulaeva[17], S H Nasyrov[17], V S Navotny[18], J Nystrand[11], G I Orlova[13], I Otterlund[11], H S Palsania[7], N G Peresadko[13], N V Petrov[17], V A Plyushchev[15], D A Qarshiev[17], W Y Qian[19], Y M Qin[10], R Raniwala[7], S Raniwala[7], N K Rao[8], V M Rappoport[13], J T Rhee[12], N Saidkhanov[18], N A Salmanova[13], L G Sarkisova[20], V R Sarkisyan20, G S Shabratova[6], T I Shakhova[1], S N Shpilev[18], D Skelding[16], K Söderström[11], Z I Solovjeva[15], E Stenlund[11], E L Surin[18], L N Svechnikova[18], K D Tolstov[6], M Tothova[9], M I Tretyakova[13], T P Trofimova[17], U Tuleeva[17], S Vokal[6,9], H Q Wang[19], Z Q Weng[5], R J Wilkes[16], Y L Xia[5], G F Xu[2], D H Zhang[10], P Y Zheng[2], S I Zhochova[18], and D C Zhou[19]

1) Alma Ata, Inst. of High Energy Physics, Kazakhstan
2) Beijing, Academica Sinica, People's Republic of China
3) Berkeley, Lawrence Berkeley Lab, USA
4) Chandigarh, Panjab University, India
5) Changsha, Hunan Education Institute, People's Republic of China
6) Dubna, JINR, Russia
7) Jaipur, University of Rajasthan, India
8) Jammu, University of Jammu, India
9) Kosice, Safarik University, Czechoslovakia
10) Linfen, Shanxi Normal University, Peoples Republic of China
11) Lund, University of Lund, Sweden
12) Marburg, Philipps University, Germany
13) Moscow, Lebedev Institute, Russia
14) Ottawa, NRC, Canada
15) St Petersburg, V G Khlopin Radium Institute, Russia
16) Seattle, University of Washington, USA
17) Tashkent, Institute of Nuclear Physics, Uzbekistan
18) Tashkent, Physical-Technical Institute, Uzbekistan
19) Wuhan, Hua-Zhong Normal University, People's Republic of China
20) Yerevan, Physical Institute, Armenia

Abstract: The energy and centrality dependence of local particle pseudorapidity densities as well as validity of various parametrizations of the distributions are examined. The dispersion, σ, of the rapidity density distribution of produced particles varies slowly with centrality and is 0.80, 0.98, 1.21 and 1.41 for central interactions at 3.7, 14.6, 60 and 200 A GeV incident energy, respectively. σ is found to be independent of the size of the interacting system at fixed energy. A novel way of representing the window dependence of the multiplicity as normalized variance versus inverse average multiplicity is outlined.

PACS numbers: 12.38.Mh, 12.40.Ee and 25.70.Np

1. Introduction

Analysis of multiparticle production in nucleus-nucleus interactions has been revitalized in quest of possible existence of a Quark-Gluon-Plasma (QGP). A key parameter in the QGP search is the local charged particle density ρ, since it can be related to the energy density. New insight can be gained, fruitful for predictions on future accelerator based experiments, by examining how ρ varies with incident energies, projectile and target masses and global multiplicity. The dispersion, σ, of the charged particle density distributions is of interest also for model comparisons. Here both global and local multiparticle production have been studied as a function of varying size of a centrally placed rapidity window.

Two parametric representations of the multiplicity distributions have had particularly widespread usage: The Negative Binomial[1,2,3,4] (NB) and the Gaussian[5,6,7,8] (GA) distributions. The NB regularity have been found in hadronic, leptonic and semileptonic processes. NB distribution can arise in physical processes like stimulated emission, cascade processes and for certain jet fragmentation processes in perturbative QCD[9]. The GA distributions have been applied to transverse-energy[6] and charged-particle multiplicity distributions [5,8] in large rapidity windows for central nucleus induced nuclear interactions supposedly by virtue of the Central Limit Theorem.

2. Experimental Techniques

2.1 The Exposures

The experimental data used in this investigation is collected either from horizontally exposed conventional emulsion stacks or from vertically exposed chambers [10,11]. The exposures took place at CERN, BNL and DUBNA during the period 1986-1989. At the CERN exposure a kicker magnet was used to switch off the ^{32}S beam when a preset integrated flux of $\Phi \simeq 25000$/spot (spotsize ~ 4 cm^2) was obtained. The flux was measured with two plastic scintillators in the beam.

2.1.1 Horizontal Exposure

The horizontally (H) exposed stacks consisted each of 30 NIKFI BR-2 emulsion plates with a sensitivity for minimum ionizing particles of typically 30 grains per 100 μm. The interactions were found by along-the-track scanning which has a very high detection efficiency. The shower particles are singly charged particles with $\beta > 0.7$ and the target-associated particles, grey and black, are mainly knockout protons and evaporation fragments from the target. Further details on the experiment including how to separate between the track categories like showers, grey and black can be found in refs. [12].

2.1.2 Vertical Exposure

The vertical (V) technique, utilizing chambers, has been described elsewhere [10,11]. For the ^{32}S + Au exposure the emulsion chambers were additionally equipped upstream with a gold foil of 250 μm thickness immediately followed by two sheets of polysthyrene (780 μm thick) each coated with 220 μm thick emulsion layers on both sides. To select central and semicentral events we use two data sample namely $N_c = 0$ and $N_c \leq 2$. Here N_c is the number of charges found inside the fragmentation cone ($\Theta_c \sim 1.0$ mrad at 200 A GeV). A fraction of minimum bias events $F(N_c)$ corresponds to a given value of N_c and can be calculated from:

$$F(N_c) = N(N_c)/N(\text{Min-Bias}) = (N(N_c)\cdot A)/(\rho_{Au}\cdot d\cdot N_A\cdot \Phi\cdot \sigma_r) \qquad (1)$$

For σ_r we use the geometrical cross section estimated to be 4.18 Barn, ρ_{Au} is the density of Au, A the mass number of Au, d the thickness of the foil (d = 250 μm) and N_A is the Avogadro's number.

We estimate, that the two event selections corresponds to 7% (N_c=0) and 20% ($N_c \leq 2$) of the reaction cross section, respectively. A check with the Lund Model Fritiof[13] gives the values 8% and 21%, i.e. in good agreement. The resolution for this technique is extremely good about 0.01 units of pseudorapidity.

3. The charge flow in the forward direction

For projectile residues a forward fragmentation cone was defined by tracks with polar angles $\Theta \leq \Theta_c \simeq 0.2 / P_{Beam}$. In the analysis events with electromagnetic dissociation and elastic scattering origin have been rejected[15,17].

As a measure of the centrality of the nuclear collision we introduce the forward charge flow Q_{zD}, defined as $Q_{zD}=\Sigma Z_{frag}+n(\eta \geq \eta_{zD})$, where Z_{frag} is the charge of an observed projectile fragment with $Z \geq 2$, and $n(\eta \geq \eta_{zD})$ is the number of shower particles with $\eta \geq \eta_{zD}$, given by $\eta_{zD}=\eta_p+0.36$, where η_p is given for various incident energies in Table 1 below. The forward cone angle Θ_{zD} calculated from η_{zD} can also be found there. In Figure 1 we show $Q_{zD} \leq 6$ data, for ^{32}S+Au collisions at 200 A GeV incident energy, as histograms. For comparisons simulated data from the Lund Fritiof Model are shown as circles. As can be seen, within the Fritiof model, pseudorapidity (Figure 1a), multiplicity (Figure 1b), centrality (Figure 1c) and $\langle n_s \rangle - Q_{zD}$ correlation (Figure 1d) distributions can be adequately described.

4. Pseudorapidity Distributions

4.1 Gaussian η-distributions

In Ref[14] the shower particle pseudorapidity distributions for centrally selected events could be reasonably well represented by Gaussian (GA) distributions. In Table 1 the definition for central interactions was $Q_{zD}/Z_{Beam} \leq 1/4$. As can be seen this corresponds to 5-12 % of the minimum bias event sample, when excluding EM dissociation and elastic scattering events.

Table 1

Type	E_{inc} A GeV	η_p	# of events	# of central events (AgBr)	σ	Θ_{zD} mrad	Θ_c mrad
^{16}O+Em	3.7	2.36	1743	138 (8%)	0.80	132	44
^{16}O+Em	14.6	3.58	631	57 (9%)	0.98	39	13
^{16}O+Em	60	4.95	534	63 (12%)	1.21	10	3.3
^{16}O+Em	200	6.14	503	50 (10%)	1.41	3	1
^{28}Si+Em	14.6	3.58	875	59 (7%)	0.98	39	13
^{32}S+Em	200	6.14	917	47 (5%)	1.41	3	1

In Figure 2 we show the pseudorapidity distributions for central ($Q_{zD} \leq 2$ and $N_h > 8$) ^{16}O+AgBr events. Here N_h is multiplicity of target-associated particles, mainly knockout protons and evaporation fragments from the target. The σ in the figure is the dispersion of the Gaussian fit to the data, and can be seen to slowly increase from 0.80 to 1.41 going from incident energies of 3.7 to 200 A GeV.

In Figure 3 we show similar curves for ^{28}Si ($Q_{zD} \leq 3$) and ^{32}S ($Q_{zD} \leq 4$) induced AgBr interactions. Note that for the same incident energy σ is independent of

projectile masses. In the lower part of the figure we show the variation of σ with Q_{ZD}/Z_{Beam} for ^{32}S + ^{197}Au, ^{16}O + Em and ^{32}S + Em interactions at 200 A GeV. As can be seen there is a slight almost linear rise in σ when passing from central to peripheral interactions for all systems. This appearant rize of σ with the increasing Q_{ZD} may be attributed to the slowing down of beam protons as the centrality increases, which makes the distribution somewhat narrower for central interactions. The best linear fit to all data at 200 A GeV gives the following equation:

$$\sigma = (1.40 \pm 0.01) + (0.13 \pm 0.02)\cdot(Q_{ZD}/Z_{Beam}) \qquad (2)$$

As can be seen the density distribution for the most peripheral events is just 10% wider than the one for the most central events.

If we assume that Gaussian distributions can be used to describe the pseudorapidity distributions it is possible to relate the maximum shower particle density ρ to the total shower multiplicity n_s as follows:

$$\rho \simeq n_s/(\sqrt{2\pi}\cdot\sigma) = B\cdot n_s \qquad (3)$$

where σ is the dispersion of the Gaussian distribution. For the Gaussian fit of the experimental data the pseudorapidity region $0 < \eta < \eta_p$ was used.

By examining, how ρ varies with the total shower multiplicity n_s, one ought to get a linear relation with a slope factor = B. One would expect the slope to be fairly independent of the particular choice of projectile and target but quite dependent of the incident energy, since the width of the pseudorapidity distribution increases with energy Ref[15].

4.2 Correlation Between Local Density and Global Multiplicity

In order to investigate the possible correlation between the local charged particle density and the total shower particle multiplicity we performed Gaussian fits to the experimental data for fixed multiplicity. We then examine how the average charged particle density $\langle\rho\rangle_m$, varies with the multiplicity m. As can be seen from Figure 4 linear relations between the quantities seem to hold, for each energy, irrespective of projectile and target combinations[16]. To count produced particles only, we define the quantity $m = n_s - Z_p + Q_{ZD}$ from the shower particles n_s, and Z_p the projectile charge (Z_p=8, 14 and 16 for ^{16}O, ^{28}Si and ^{32}S, respectively).

Table 2

E_{inc} A GeV	Y_{proj}	Slope from Eqs. 3	Slope from linear fit
3.7	2.28	0.50	0.57 ± 0.03
14.6	3.50	0.41	0.42 ± 0.02
60.	4.87	0.33	0.35 ± 0.01
200.	6.06	0.28	0.27 ± 0.01

A straight line fit to the three experimental data sets give slope factors B which can be found in Table 2. Observe that the slopes can be reproduced utilizing equation 3 and using the dispersions σ quoted in Table 1. Note also that this empirical proportionallity relation between local charged particle density as a function of global produced particle multiplicity can be used for heavy-ion reactions in general provided that the energy dependence of the

slopefactor is taken into account.

In Figure 5 we visualize the energy dependence of the slopefactor B, from Equation 3, as a function of $1/Y_{proj}$. Here, Y_{proj} is the rapidity of the beam. Also shown is a least square fit to the data of the formula:

$$B = \alpha + \beta \cdot (1/Y_{proj}) \qquad (4)$$

The parameters α and β were found to be $\alpha = 0.10 \pm 0.02$ and $\beta = 1.14 \pm 0.07$ and can be used for interpolations in the kinetic energy intervall 3.7 to 200 A GeV.

In Figure 6 we show the peak position of the η-distribution, as obtained from Gaussian fits of O + Em reactions from various energies, as a function of Q_{ZD}. As can be seen a rather weak dependence on centrality is found(at most 10%). It is reasonable to conclude that the dependence has its origin in the nuclear overlap geometry, since the same trend is observed at various energies. The peak position, η_{peak}, is never strongly deviating from what is expected for nucleon-nucleon collisions($\eta_{peak} \sim \eta_p/2$). In Table 3 we show the slopes obtained from linear fits like $\eta_{peak} = \kappa \cdot Q_{ZD} + \omega$. Observe that the slopes seem to be independent of incident energies.

Table 3

E_{inc} A GeV	Y_{proj}	Slope κ linear fit	Intercept ω linear fit
3.7	2.28	0.050±0.011	1.27 ± 0.05
14.6	3.50	0.042±0.012	1.74 ± 0.06
60.	4.87	0.036±0.015	2.43 ± 0.07
200.	6.06	0.044±0.016	2.98 ± 0.08

5. Multiplicity Distributions

5.1 Global Characteristics

The general shape of the minimum bias multiplicity distribution shows a peak at low multiplicity with a steep fall off with increasing multiplicity, followed by a plateau and shoulder and a fast declining tail at the highest multiplicity.

The mean and dispersion of the shower particle multiplicity distributions, for minimum bias O+Em interactions of 3.7, 14.6, 60 and 200 A GeV incident energies, are shown in Table 4.

This agrees inside error bars with values quoted earlier for less statistics[17]. Note that the ratio $\sigma/\langle n_s \rangle$ is practically constant and close to unity for the three higher energies which reflects asymptotic multiplicity scaling. However, there is significant deviation at 3.7 A GeV which can be attributed to the increasing weight of the fragmentation regions at this energy. For central O+AgBr interactions, see Table 5, scaling is present even at 3.7 A GeV and the quotient $\sigma/\langle n_s \rangle$ is found to be close to 0.3.

Table 4

O+Em, Minimum Bias

E_{inc} A GeV	$\langle n_s \rangle$	σ_n	$\sigma_n/\langle n_s \rangle$
3.7	11.6±0.2	9.2±0.2	0.79±0.02
14.6	22.1±0.8	20.6±0.7	0.93±0.03
60.	40.6±2.2	41.6±1.9	1.02±0.05
200.	58.1±2.8	61.5±2.5	1.06±0.04

Table 5

O+AgBr, Central ($Q_{ZD}/Z_{Beam} \leq 1/4$, $N_h > 8$)

E_{inc} A GeV	$\langle n_s \rangle$	σ_n	$\sigma_n/\langle n_s \rangle$
3.7	26.4±0.8	8.3±0.8	0.31±0.03
14.6	61.7±2.3	17.1±2.1	0.28±0.03
60.	106. ±4.6	41.2±4.5	0.39±0.05
200.	174. ±7.0	49.1±6.5	0.28±0.04

5.2 Effects of Repeated Intranuclear Collisions

Let us define P as the number of participating nucleons. In Figure 7 we show the n_s/P as a function of centrality parameter Q_{ZD}/Z_{Beam} for ^{32}S+Em, ^{32}S+^{197}Au and ^{16}O+Em interactions at 200 A GeV. The number of participants was recorded from Fritiof simulations, but can in principle also be estimated from geometrical overlap assumptions. For peripheral interactions the values are close to the expected yield from pp collisions (corrected for slow protons) at corresponding incident energy i.e. $(n_{ch}-0.5)/2$ with n_{ch} = 7.68 [18]. An interesting result is the increase in n_s/P with centrality. In central nuclear interactions individual nucleons can do successive collisions and thereby gain in excitation of the spanned string. For comparisons we have also included the outcome from the Fritiof simulations. As can be seen there is a close resemblance between our data and the model calculations.

5.3 Predictions for Pb+Pb collisions

In Figure 8 we show the variation of $\langle m \rangle/P$ with n_{ch}, the charged particle multiplicity in pp collisions, for incident energies of 3.7, 14.6, 60 and 200 A GeV and for ^{16}O + Em, ^{28}Si + Em and ^{32}S + Em. As can be seen a straight line $\langle m \rangle/P = 0.734 \cdot n_{ch} - 1.44$, can be used to represent the data[19].

In Figure 9 and Figure 10, simulated data from the Venus and Fritof model are compared with experimental data from ^{16}O+Ag and ^{32}S+Au interactions at 200 A GeV. There seem to be a slight excess in the Venus model at high multiplicity.

The straight line fit of Figure 8 makes it possible to estimate $\langle m \rangle$ for near head-on central ^{208}Pb+^{208}Pb collisions where all nucleons are expected to participate i.e. P=416. An interpolation in Figure 8 gives $\langle m \rangle/P$ = 3.84 at 160 A GeV and therefore we expect the multiplicity $\langle m \rangle$ to be about 1600 charged particles. The dispersion of the pseudorapidity distribution will be $\sigma \simeq 1.38$

(corresponding to a slopefactor B ~ 0.29 from Figure 5). The peak position (160 A GeV) is calculated from $\eta_{peak} \simeq Y_{proj}/2 + 0.25 \simeq 3.17$, which is obtained from η-peak values for peripheral collisions in Figure 6. We have chosen the peripheral collisions in Figure 6, since they are the most symmetrical ones. The phenomenologically predicted η-distribution of a central $^{208}Pb+^{208}Pb$ collision is given in Figure 11. The charged particle density is about $\rho = 460$ which corresponds to an average energy density of about 2 GeV/fm^3.

5.4 Stochastic Emission

In Ref.[20,21] it was shown that if, in a given event particles are produced without correlation in the phase space, then the normalized variance $\Omega = (\sigma/\langle n\rangle)^2$ is given by:

$$\Omega = F_2 - 1 + 1/\langle n\rangle \tag{5}$$

where $\langle n\rangle$ is the mean multiplicity inside a rapidity window and F_2 is the second scaled factorial moment [22]. An analysis in terms of the scaled factorial moment for S+Au interactions at 200 A GeV is rather recently reported in Ref. [23]. For large $\langle n\rangle$ an approximate linear relationship between σ and $\langle n\rangle$ for different windows in rapidity is expected. However, for the NB distribution the normalized variance $\Omega =$ is given by:

$$\Omega = 1/k + 1/\langle n\rangle \tag{6}$$

Equation 6 reveals that one might study Ω as a function of $1/\langle n\rangle$. This should yield a straight line with slope unity which has an intercept of $1/k$ as $1/\langle n\rangle \rightarrow 0$. In this way $1/k$ is related to F_2 the second scaled factorial moment as: $1/k = F_2 - 1$. Since any stochastic particle production process exhibits a linear dependence between Ω and $\langle n\rangle^{-1}$ and the k-value can be determined from the intercept it seems natural to constrain the k value to be the same to test the validity of the NB distributions. To illustrate this we have in Figure 12 plotted σ as a function of $\langle n_s(\delta\eta)\rangle$ for three different centrality cuts of $^{16}O+Em$ interactions at 200 A GeV. As can be seen in the inset of Figure 12 we obtain straight lines in all three cases. The k-values determined from the slopes are found to be k=3 (N_h>8), k=4 (N_h>15) and k=7 (N_h>26). Here N_h is multiplicity of target-associated particles, mainly knockout protons and evaporation fragments from the target. If a NB distribution is the correct parametrization these k-values should describe the distribution and should not be a free parameter.

In Figure 12 we have also studied how well the NB distributions can represent local multiplicity data for various window sizes. For this purpose a centrally placed window, around nucleon-nucleon centre-of-mass, was used. This large window was then subdivided into smaller bins according to the recipe $\delta\eta = \Delta\eta/2^{m-1}$, m=1,..,6. All bins inside the window was used to increase statistics. Typical resolution in pseudorapidity with the horizontal exposure technique is about 0.1 units thereby setting a lower limit on window size.

Utilizing the above mentioned k-values we have calculated χ^2/DOF for the representation of data by NB distributions as a function of binsize $\delta\eta$. As can be seen in Figure 12, only for well defined central interactions (7% of reaction cross section), can data be represented by NB distribution for a wide interval of window sizes. In the following NB analysis only sharply defined central events will be used.

5.5 Number of Sources for Particle Production

Let us assume that we have k sources which all contributes to the charged

multiplicity spectrum according to the same geometric distribution:

$$P(n)=p^n\cdot(1-p) \tag{7}$$

One can easily show, by inductive proof, that the convolution of k such sources will give a NB distribution. In Figure 13 we show a novel way of representing the data with normalized variance as a function of inverse mean multiplicity. The intercept will according to Equation 6 be equal to 1/k. The merit of this representation is that one extrapolates to infinite mean multiplicity and is presumably free from binsize effects. However as we will show below effects of density fluctuations inside the projectile and target nuclei prohibit the direct interpretation of k as the number of sources. We will now consider a more realistic case where we have a distribution of sources υ, $P(\upsilon)$ and that each source contributes to the charged multiplicity spectrum according to the same geometric distribution. In this way we can allow for difference in number of sources from event to event due to density fluctuations and impact parameter variation for a given central trigger. Let us denote by $\langle m\rangle$ the mean multiplicity of a single source. It is then straightforward to show that:

$$\langle n\rangle=\Sigma P(\upsilon)\cdot\upsilon\langle m\rangle=\langle\upsilon\rangle\cdot\langle m\rangle \tag{8a}$$

$$\langle n^2\rangle=\Sigma P(\upsilon)\cdot(\upsilon^2\cdot\langle m\rangle^2+\upsilon\cdot\langle m\rangle^2+\upsilon\cdot\langle m\rangle)= \langle\upsilon^2\rangle\cdot\langle m\rangle^2+\langle\upsilon\rangle\cdot\langle m\rangle^2+\langle\upsilon\rangle\cdot\langle m\rangle \tag{8b}$$

From the expression above the following useful expression can be obtained:

$$\lim_{(1/\langle n\rangle)\to 0} \Omega(n)=\Omega(\upsilon)+1/\langle\upsilon\rangle=1/k \tag{9}$$

In figure 13 two straight line fit have been performed for the two event selections. From the fitted line we obtain $1/k = 0.065 \pm 0.013$ and 0.080 ± 0.012 for $N_c=0$ and $N_c\leq 2$, respectively. To be able to estimate the number of sources we have used $\Omega(\upsilon)$ from the Fritiof Model yielding values of 0.0215 and 0.0398, respectively for the two event samples. The normalized variance is supposingly not so sensitive to specific model assumptions. From their numbers we estimate the number of sources to be 23 ± 10 and 24 ± 11 respectively. This number of sources is much smaller than what is expected from spectator-participant considerations and a straight forward interpretation can not easily be given.

5.5.1 NB (Negative-Binomial Distribution)-parametrization

For completeness we give here the NB distribution used which is entirely defined by two parameters $\langle n\rangle$ and k as:

$$P(n) = \binom{n+k-1}{n} \cdot p^n \cdot (1-p)^k \tag{10}$$

where $p=\langle n\rangle/(\langle n\rangle+k)$. For negative k a Binomial Distribution is obtained and when $1/k \to 0$ one obtains a Poisson Distribution. Thus the NB distribution is quite versatile. As was discussed above to be consistent k is expected to be independent of window size $\delta\eta$ for stochastic emission.

5.5.2 GA (Gaussian Distribution)-parametrization

In Figure 14 we exhibit unity normalized charged particle multiplicity distributions for $^{32}S + {}^{197}Au$ interactions at 200 A GeV. Four different sizes of the pseudo-rapidity window are displayed and Gaussian fits have been performed and superimposed in the figure to guide the eye. As can be seen the Gaussian di-

stribution can well describe the data for large down to medium sized η-windows. Table 6 compares fits to NB and GA distributions. One learns from the table that present statistics can not discriminate between the two representations for large and medium binsizes.

Table 6

	NB Distribution			GA Distribution		
δη	$\langle n_s \rangle$	K	χ^2/DOF	$\langle n_s \rangle$	σ_{ns}	χ^2/DOF
2.	220. ± 22.	22 ± 2	0.61	220. ± 20.	44.7 ± 4.5	0.55
1.	116. ± 10.	17 ± 1	0.58	111. ± 10.	29.7 ± 2.1	0.52
0.5	56.5 ± 5.1	14 ± 1	1.8	53.4 ± 2.7	15.8 ± 0.15	1.4
0.25	27.7 ± 2.2	15 ± 1	1.7	26.4 ± 0.5	8.58 ± 0.17	1.1
0.125	13.3 ± 0.7	16 ± 2	2.6	13.1 ± 0.1	4.91 ± 0.09	1.8
0.0625	6.80 ± 0.5	15 ± 1	2.7	6.47 ± 0.1	3.17 ± 0.06	3.4
0.0313	3.36 ± 0.2	15 ± 1	2.8	3.04 ± 0.1	2.15 ± 0.01	10.
0.0156	1.58 ± 0.1	12 ± 1	2.0	1.48 ± 0.1	1.50 ± 0.14	62.

5.6 Relative Information Entropy of Particle Production

5.6.1 Entropy

It has been argued that the multiplicity distributions can be used to calculate the information entropy[24] of the collisions defined as:

$$S = -\sum_{n=1}^{N} P(n)\ln P(n), \qquad \sum_{n=1}^{N} P(n)=1 \tag{11}$$

where P(n) is the unity normalized inclusive multiplicity distribution and N is the maximum multiplicity. As can be seen the entropy can vary from 0, if a certain multiplicity has probability 1, upto the value ln (N), when all probabilities are equally probable and equal to 1/N. Here N can be estimated to be:

$$N = (\sqrt{s} - 2m_N c^2)/(m_\pi c^2) \tag{12}$$

To be able to do intercomparisons at different energies and projectile and target combinations a relative quantity has been defined as[25]:

$$R = S/S_{max} \tag{13}$$

In Figure 15 a we show a comparison of relative entropy in full phase space for a minimum bias samples of ^{16}O+Em interactions at three incident energies. The solid line show outcome from Fritiof simulations. A relative entropy value of about 0.6 is obtained with no noticeable energy dependence. In Figure 15 b we show the relative entropy R as a function of scaled pseudorapidity window size $\xi = \eta_c/\eta_{max}$ for ^{16}O and ^{32}S induced interactions at 200 A GeV. The dot-dashed and dashed curves represent outcome from Fritiof calculations. As can be seen experimental data agree within errors with Fritiof predictions.

5.6.2 Scaling in global n_s

In an earlier paper[17] we explored asymptotic scaling in the multiplicity istributions. We found a scaling distribution $f(x)=P(n)\cdot\langle n\rangle$ where $x=n/\langle n\rangle$ for

the energies 14.6, 60 and 200 A GeV incident energies. P(n) is the unity normalized multiplicity distribution. The maximum multiplicity N_{max} is then given by $N_{max} = K \cdot \langle n \rangle$ for a given energy. K would thus change only weakly with energy.

5.6.3 Expected entropy from the scaling distributions

We now assume that asymptotic scaling is present and calculate from Eqs. 11 and 13 the information entropy:

$$R_{max} = -\Sigma P(n) \cdot \ln P(n)/\ln(N_{max}) \simeq -\int f(x) \cdot \ln (f(x)/\langle n \rangle)\, dx/\ln(N_{max}) =$$

$$= (\ln \langle n \rangle - \int f(x) \ln f(x)\, dx)/(\ln \langle n \rangle + \ln K) =$$

$$= (\ln \langle n \rangle + \ln \Psi)/(\ln \langle n \rangle + \ln K) \qquad (14)$$

where

$$\ln \Psi = -\int f(x) \ln f(x)\, dx \qquad (15)$$

Due to scaling we would expect Ψ to have a much weaker energy dependence than $\langle n \rangle$, and also K would change only weakly with energy. Experimentally we see that $R < 1$ and thus $\ln \Psi < \ln K$. We can thus expect that R will grow with increasing energy and asymptotically become 1. It therefore seems that the concept is insensitive and perhaps of limited use for the QGP search.

5. Discussions and Conclusions

We have outlined phenomenological ways of parametrizing energy and centrality dependence of pseudorapidity distributions. It has predictive power in that sense that the outcome of central Pb + Pb collisions at 160 A GeV can be estimated, which is of interest in the CERN/SPS perspective. The width of the pseudorapidity spectra, σ is found to increase with energy as $\ln (E_{proj})$ but found to be independent of size of the interacting system. Furthermore a weak dependence on centrality is observed. From the behaviour of the variation of peak-position with Q_{ZD} with almost the same linear decrease for all energies with centrality, and from the linear relation between $\langle m \rangle/P$ and n_{ch} it is natural to conclude that the geometry of the nuclear collisions and the number of participating nucleons, play an important rôle in the particle production. In order to get as small geometrical fluctuations as possible on the multiplicity spectra one needs to restrict oneself to well defined central event samples. Even so, due to density fluctuations and variation in impact parameter of the collision, the width of the source distribution can never be neglected. We have outlined a recipe to examine the data and to estimate the number of sources. Our conclusion is that a description of the multiplicity distribution by NB distribution is limited and seem only to be relevant for sharply defined centrality and rapidity window size cuts.

Acknowledgements: We like to express our thanks to the CERN staff at the PS and SPS. We are also extremely thankful for the contributions given by the scanning-measuring staffs within the collaboration. The financial support from the Swedish NFR, the International Seminar in Uppsala, the German Federal Minister of Research and Technology, Third World Academy of Science (TWRG-277), the Department of University Grants Commision of India, the National Natural Science Foundation of China, the Distinguished Teacher Foundation of the State Education Commision of China, the Fok Ying Tung Education Foundation and finally USDOE and NSF in USA are gratefully acknowledged.

References

[1] A. Giovannini and L. Van Hove, Z. Phys. **C30**, 391 (1986)
[2] NA5 Collaboration F. Dengler et al, Z. Phys. **C33**, 187 (1986)
[3] A. Giovannini and L. Van Hove, CERN-TH.4894/87
[4] A. Giovannini and L. Van Hove Acta Phys. Pol. **B19**, 495 (1988)
[5] I. Otterlund et al, Proc. Int. Conf. on Physics and Astrophysics of Quark Gluon Plasma, Bombay, India 1988 B. Sinha, S. Raha, (eds.) Singapore: Word Scientific
[6] NA34 Collaboration (HELIOS) T. Akesson et al, Z. Phys. **C38**, 383 (1988)
[7] G. Baym, G. Friedman and I. Sarcevic, Phys. Lett. **B219**, 205 (1989)
[8] WA80 Collaboration, R. Albrecht et al, Z. Phys. **C45**, 31 (1989)
[9] A. Giovannini, Nucl. Phys. B161, 429 (1979)
[10] EMU01 Collaboration: M. I. Adamovich et al, Phys. Lett. **B201**, 397 (1988)
EMU01 Collaboration: M. I. Adamovich et al, Phys. Lett. **B227**, 285 (1989)
[11] S. Garpman et al, Nucl. Instr. Meth. **A269**, 134 (1988)
[12] EMU01 Collaboration: M. I. Adamovich et al, Phys. Lett. **B234**, 180 (1990)
[13] B. Nilsson-Almqvist and E. Stenlund, Com. Phys. Comm. **43**, 387 (1987)
[14] EMU07 Collaboration: H. von Gersdorff et al, Phys. Rev. **C39**, 1385 (1989)
[15] EMU01 Collaboration: M. I. Adamovich et al, Phys. Rev. Lett. 62, 2801 (1989)
[16] EMU01 Collaboration: I. Otterlund et al, International Symposium on High-Energy Nuclear Collisions & Quark Gluon Plasma, Kyoto, Japan, World Scientific, 180 (1991).
[17] EMU01 Collaboration: M. I. Adamovich et al, Phys. Lett. **B223**, 262 (1989)
[18] E. Albini et al, Il Nuovo Cim **32A**, 101 (1976)
[19] EMU01 Collaboration: M. I. Adamovich et al, Mod. Phys. Lett. **A5**, 169 (1990)
[20] EMU01 Collaboration: M. I. Adamovich et al, Phys. Lett. **B242**, 512 (1990)
[21] T. C. Awes ORNL Preprint, To appear in Phys. Rev. D Jan (1990)
[22] A. Bialas and R. Peschanski, Nucl. Phys. **B273**, 703 (1986)
Nucl. Phys. **B308**, 857 (1988)
[23] EMU01 Collaboration: M. I. Adamovich et al, Phys. Rev. Lett. 65, 412 (1990)
[24] V. Simak, M. Sumbera and I. Zborovsky, Phys. Lett. **B206**, 159 (1988)
[25] X. Cai, D. C. Zhou, J. Zhou and Z. Zhou, Wuhan preprint HZPP-90-3 (Wuhan,China 1990)

Figure Captions

Figure 1

Histograms showing central ($Q_{ZD} \leq 6$) data from ^{32}S + Au interactions at 200 A GeV. Comparisons with the Lund Fritiof model on pseudorapidity (a), multiplicity (b), Q_{ZD}-centrality (c) and $\langle n_s \rangle$-Q_{ZD} (d) correlation distributions. For the multiplicity distributions (b) filled circles show minimum bias data.

Figure 2

Pseudorapidity distributions for central ^{16}O + AgBr interactions at 3.7(a), 14.6(b), 60(c) and 200 A GeV(d). Gaussian fits (solid lines) are superimposed. The dispersions σ of the Gaussian distributions are given for each energy.

Figure 3

Pseudorapidity distributions for central ^{28}Si + AgBr and ^{32}S + AgBr at 14.6(a) and 200 A GeV(b), respectively. Gaussian fits (solid lines) are superimposed. In (c) the variation of the dispersion σ, for the Gaussian fits with the centrality parameter Q_{ZD}/Z_{Beam} is shown. The data are for ^{32}S + ^{197}Au, ^{16}O + Em and ^{32}S + Em interactions.

Figure 4

Local shower particle density ρ as a function of global multiplicity for ^{16}O+Em at 3.7 A GeV(a), ^{16}O+Em and ^{28}Si+Em data at 14.6 A GeV(b), ^{16}O+Em data at 60 A GeV(c) and ^{16}O+Em, ^{32}S+Em and ^{32}S+Au at 200 A GeV(d). A straight line fit of the data is shown for each energy(solid line) separately.

Figure 5

The slope factor B, from equation 3, versus the inverse beam rapidity. The solid line shows a least square fit of the form: $B = \alpha + \beta \cdot (1/Y_{proj})$.

Figure 6

The position of the pseudorapidity maximum η_{Peak} as a function of Q_{ZD}. The peak position η_{Peak} is obtained from Gaussian fit to ^{16}O + Em data at 3.7, 14.6, 60 and 200 A GeV.

Figure 7

n_s per participants as a function of centrality Q_{ZD}/Z_{Beam} for ^{32}S+Em, ^{32}S+^{197}Au and ^{16}O+Em at 200 A GeV. Fritiof calculations for ^{32}S+^{197}Au (solid curve) are also shown. The value estimated from pp interactions is indicated by the dashed line.

Figure 8

$\langle m \rangle / P$ as a function of n_{ch}, the charged particle multiplicity in pp collisions, at the corresponding energy. P is the average number of participants in the reaction for ^{32}S+Em, ^{28}Si+Em and ^{16}O+Em at 3.7, 14.6, 60 and 200 A GeV.

Figure 9

ρ versus multiplicity of produced particles for the Venus (open circles) and Fritiof (filled circles) models for ^{16}O + Ag at 200 A GeV. The solid line give best fit to experimental data.

Figure 10

ρ versus multiplicity of produced particles for the Venus (open circles) and Fritiof (filled circles) models for ^{32}S + Au at 200 A GeV. The solid line give best fit to experimental data.

Figure 11

Predicted pseudorapidity distribution for central ^{208}Pb+^{208}Pb interactions at 160 A GeV.

Figure 12

(a) Straight line fit of the dispersion of shower particle multiplicity distributions versus mean multiplicity for different bin sizes in ^{16}O+ Em interactions at 200 A GeV incident energy. (b) χ^2/DOF for NB-fits to the data for various binsizes and N_h criteria.

Figure 13

Normalized variance of shower particles as a function of the inverse average multiplicity for various central pseudorapidity windows. Data used are from ^{32}S+^{197}Au interactions at 200 A GeV. Lines show N_c=0 and Nc$\leq$2. Also shown are straight line fits to the data points.

Figure 14

Shower particle multiplicity distributions for varying size of a pseudorapidity window centered around the nucleon-nucleon centre-of-mass rapidity (η_{NN} = 3.1). Gaussian fits to the data are also shown to guide the eye.

Figure 15

(a) Relative entropy in full phase space for minimum bias samples of ^{16}O+Em interactions at 14.6, 60 and 200 A GeV. Solid curve shows outcome from the Fritiof model. At lower incident energies where the model may not be applicable the line is dashed. (b) Dependence of the relative entropy with scaled pseudorapidity window size $\xi = \eta_c/\eta_{max}$ for ^{16}O and ^{32}S induced interactions at 200 A GeV with emulsion nuclei. The solid curves indicate Fritiof predictions for ^{16}O+Em and ^{32}S+Em, respectively.

Fig. 1

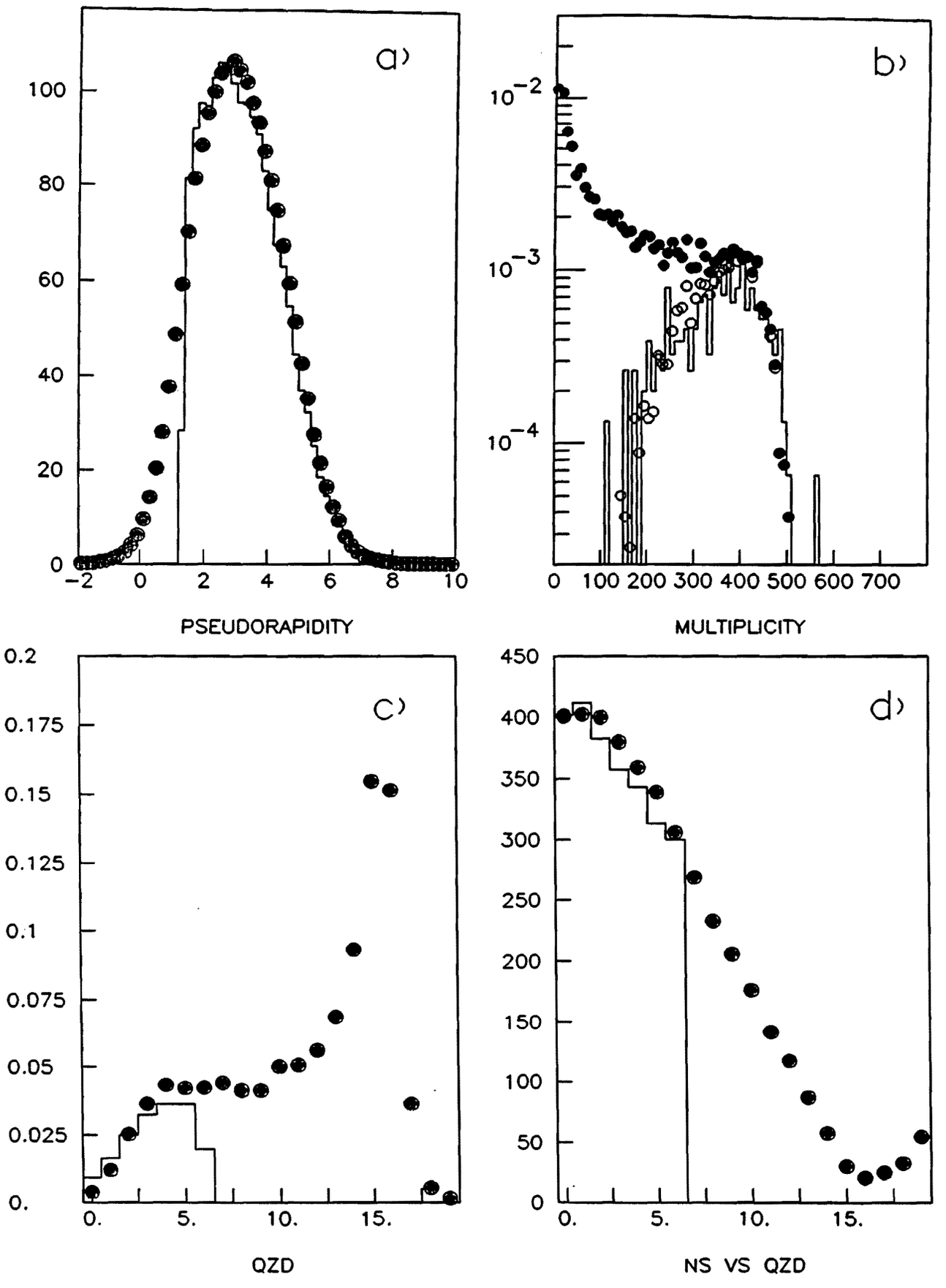
a)
100
80
60
40
20
0
−2
0
2
4
6
8
10
PSEUDORAPIDITY
b)
10^{-2}
10^{-3}
10^{-4}
0
100
200
300
400
500
600
700
MULTIPLICITY
c)
0.2
0.175
0.15
0.125
0.1
0.075
0.05
0.025
0.
0.
5.
10.
15.
QZD
d)
450
400
350
300
250
200
150
100
50
0
0.
5.
10.
15.
NS VS QZD

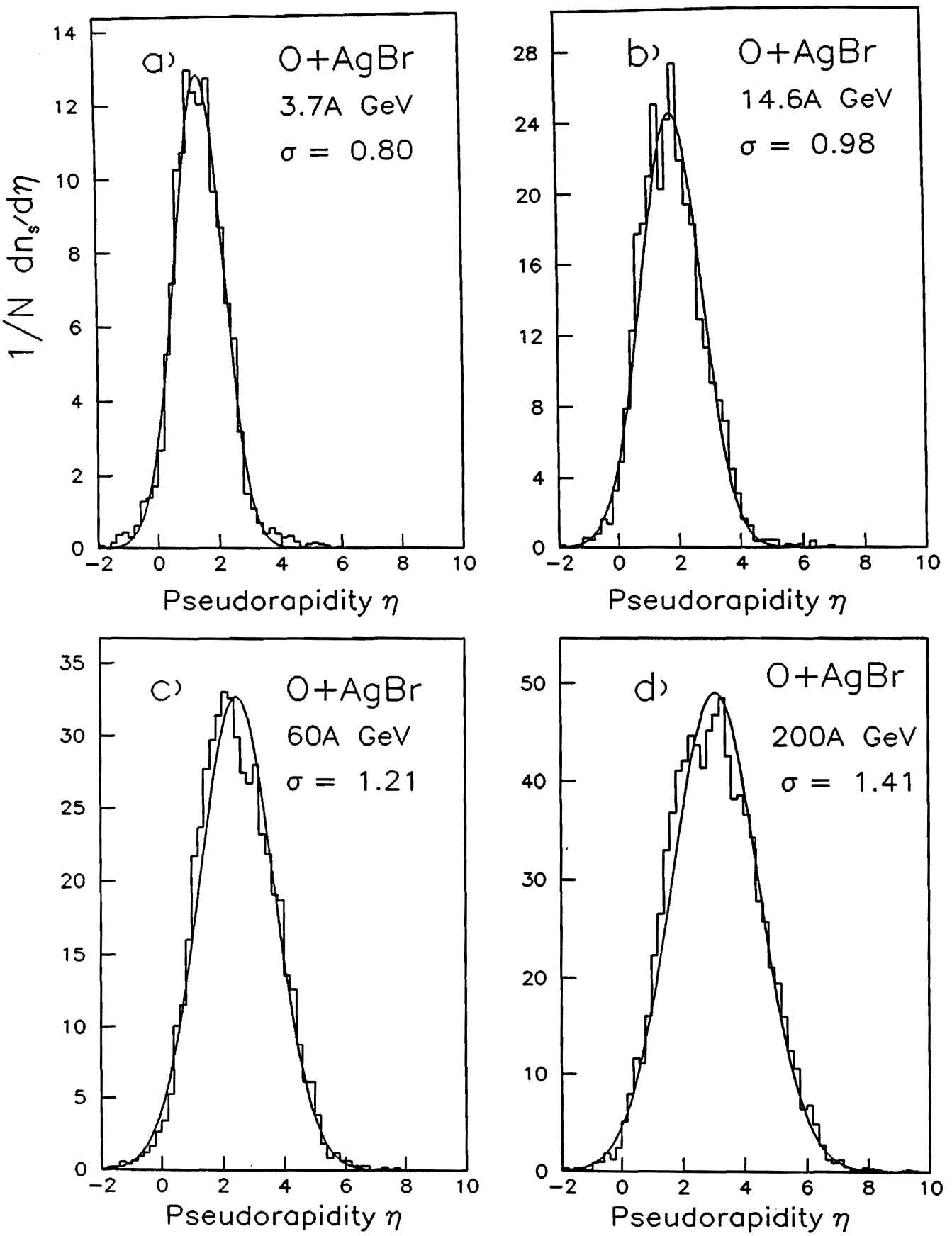
a)
O+AgBr
3.7A GeV
σ = 0.80
b)
O+AgBr
14.6A GeV
σ = 0.98
c)
O+AgBr
60A GeV
σ = 1.21
d)
O+AgBr
200A GeV
σ = 1.41
1/N dn_s/dη
Pseudorapidity η
Pseudorapidity η
Pseudorapidity η
Pseudorapidity η

Fig. 3

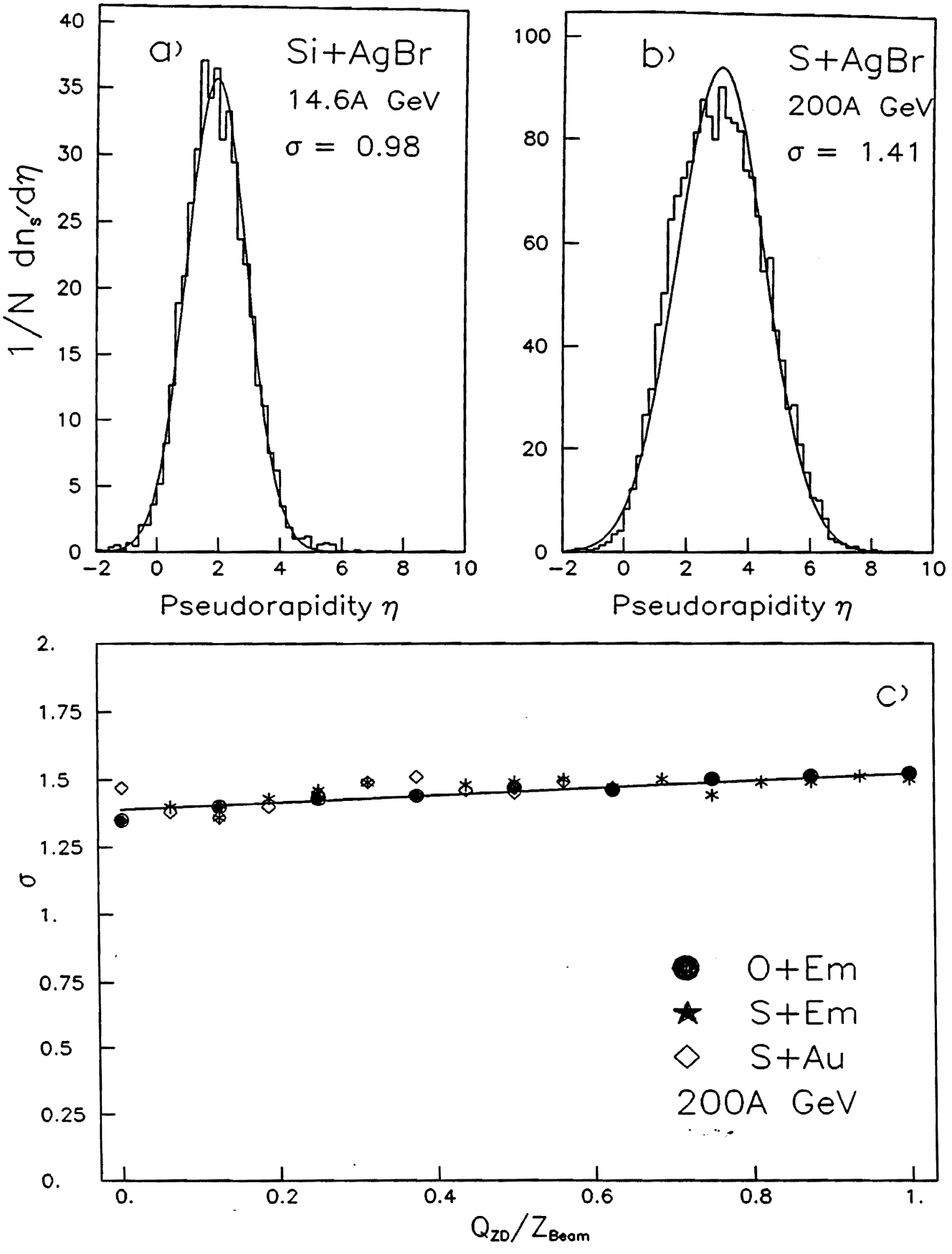
a)
Si+AgBr
14.6A GeV
σ = 0.98
1/N dn_s/dη
Pseudorapidity η
b)
S+AgBr
200A GeV
σ = 1.41
Pseudorapidity η
c)
σ
Q_ZD/Z_Beam
O+Em
S+Em
S+Au
200A GeV

Fig. 4

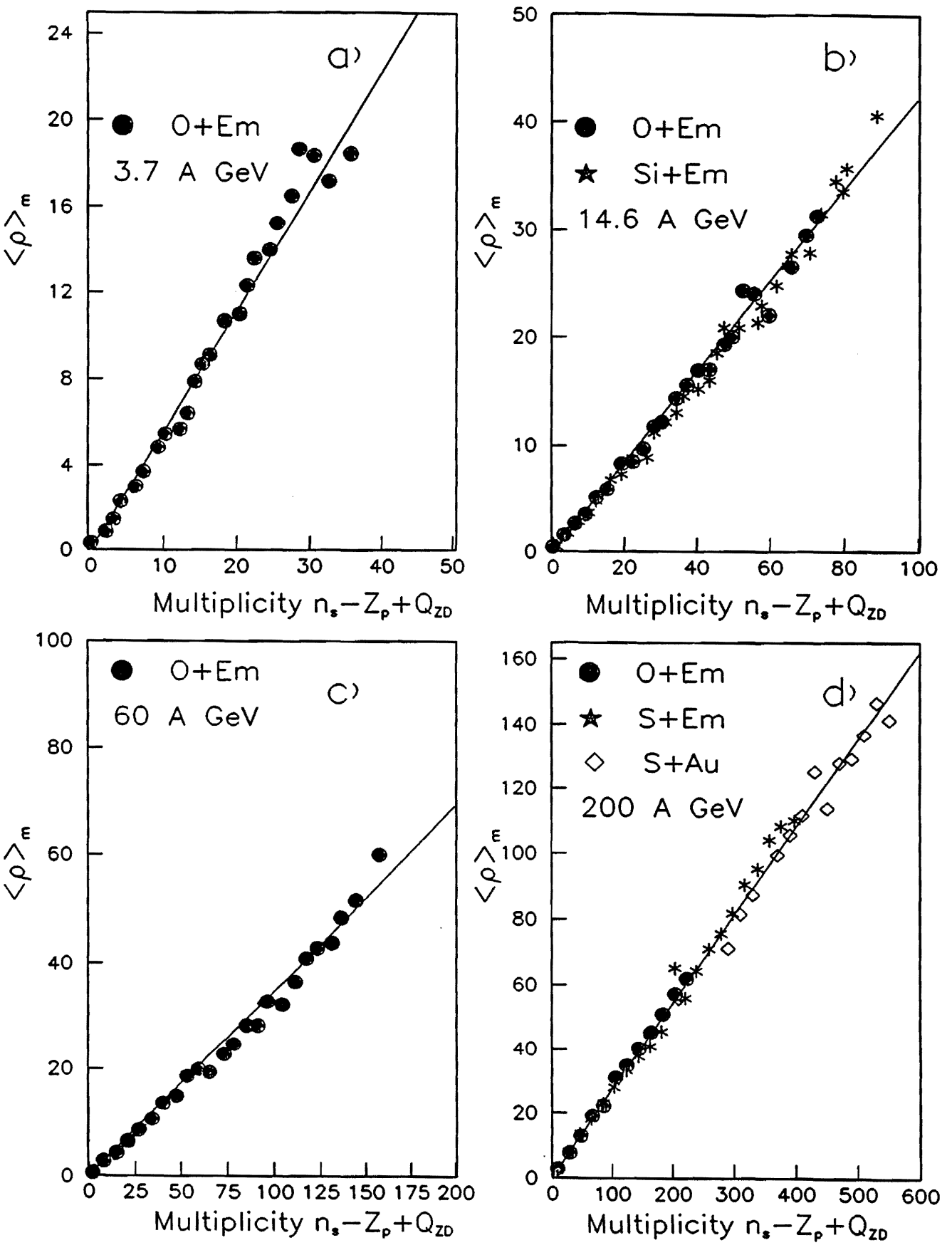
a)
O+Em
3.7 A GeV
b)
O+Em
Si+Em
14.6 A GeV
c)
O+Em
60 A GeV
d)
O+Em
S+Em
S+Au
200 A GeV
$\langle\rho\rangle^{\varepsilon}$
Multiplicity $n_s - Z_p + Q_{ZD}$

Fig. 5

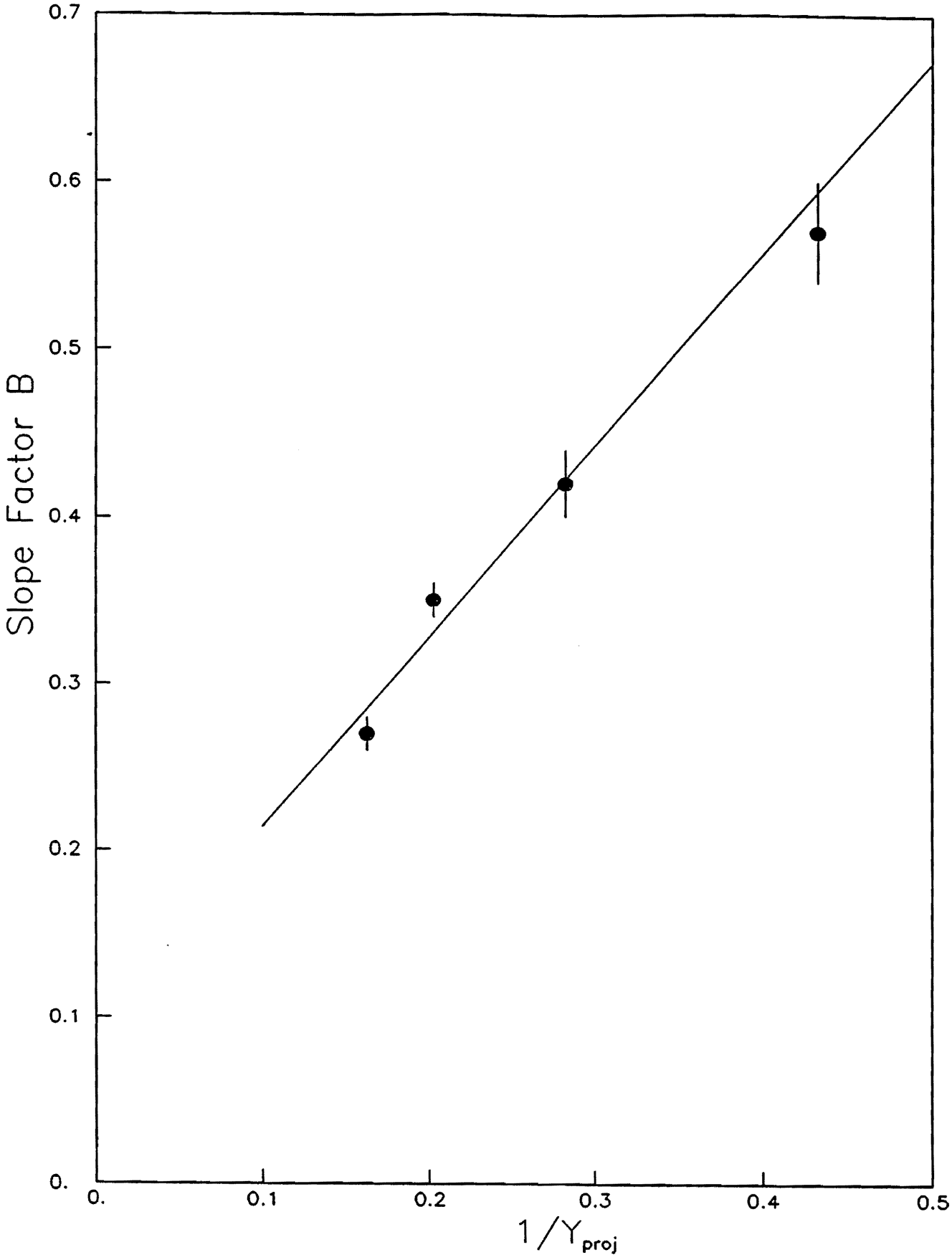

Fig. 6

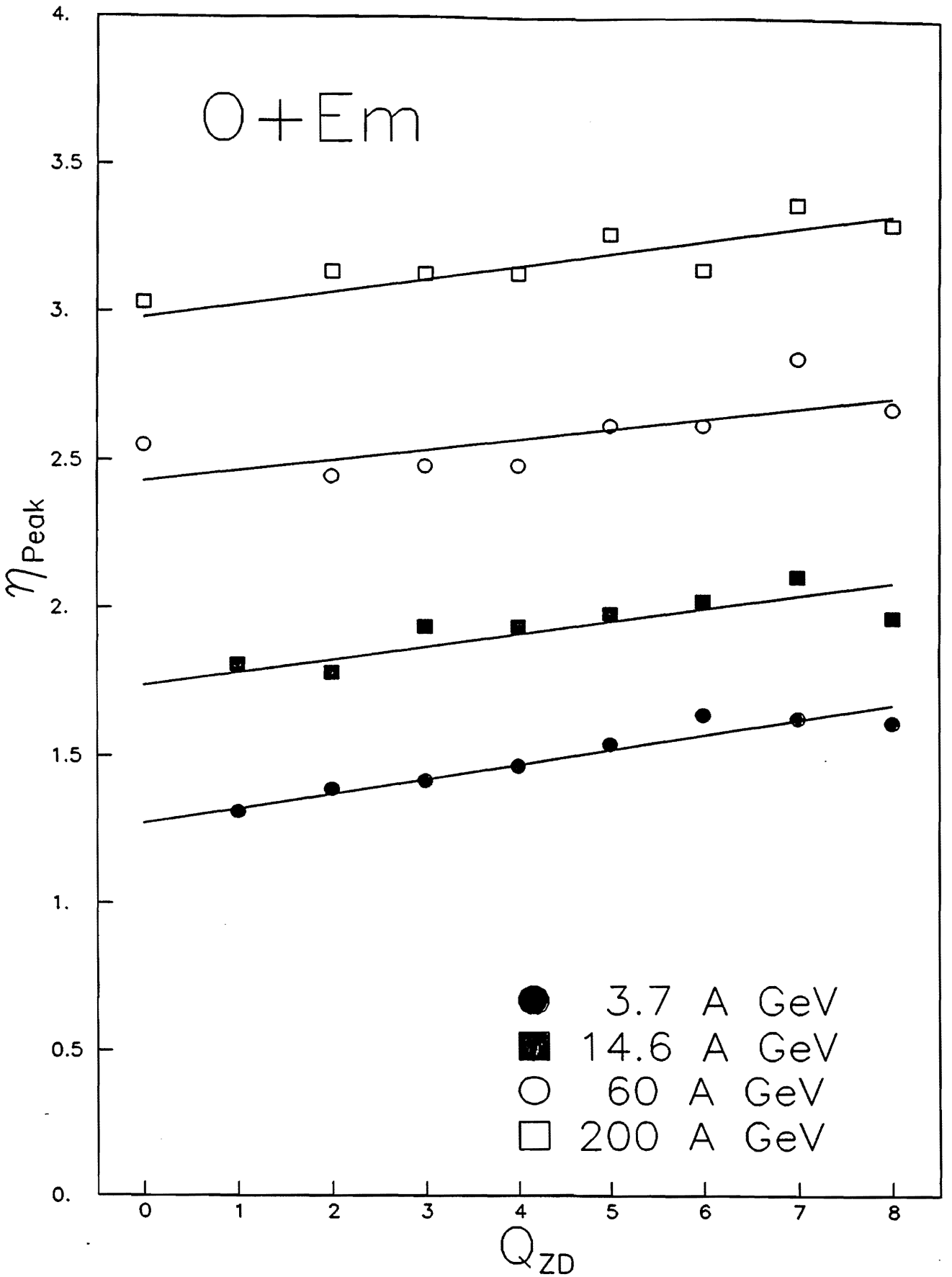
O+Em
4.
3.5
3.
2.5
2.
1.5
1.
0.5
0.
η_{Peak}
0
1
2
3
4
5
6
7
8
Q_{ZD}
3.7 A GeV
14.6 A GeV
60 A GeV
200 A GeV

Fig. 7

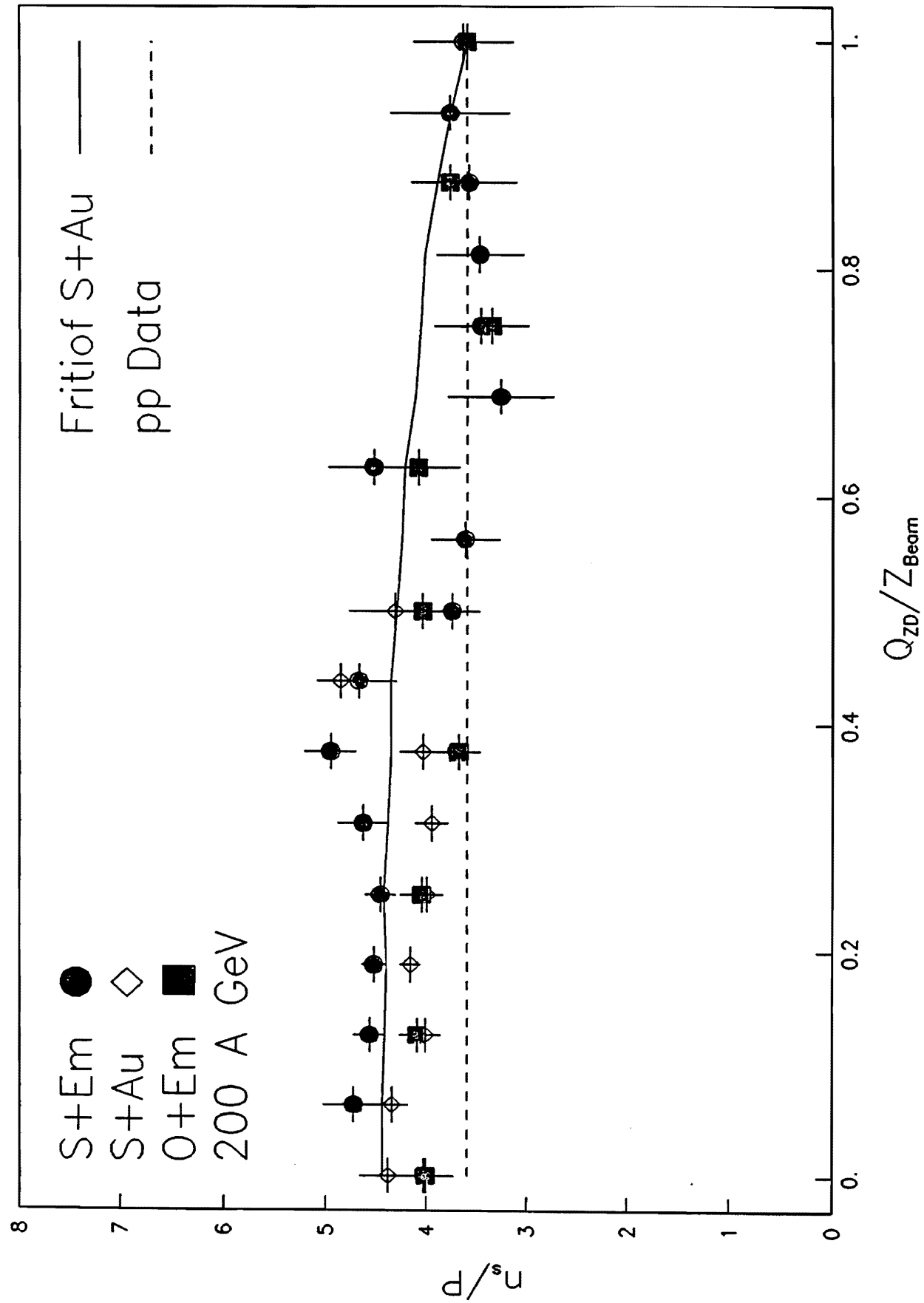
Fritiof S+Au
pp Data
S+Em
S+Au
O+Em
200 A GeV
n_s/p
Q_{ZD}/Z_{Beam}
0
1
2
3
4
5
6
7
8
0.
0.2
0.4
0.6
0.8
1.

Fig. 8

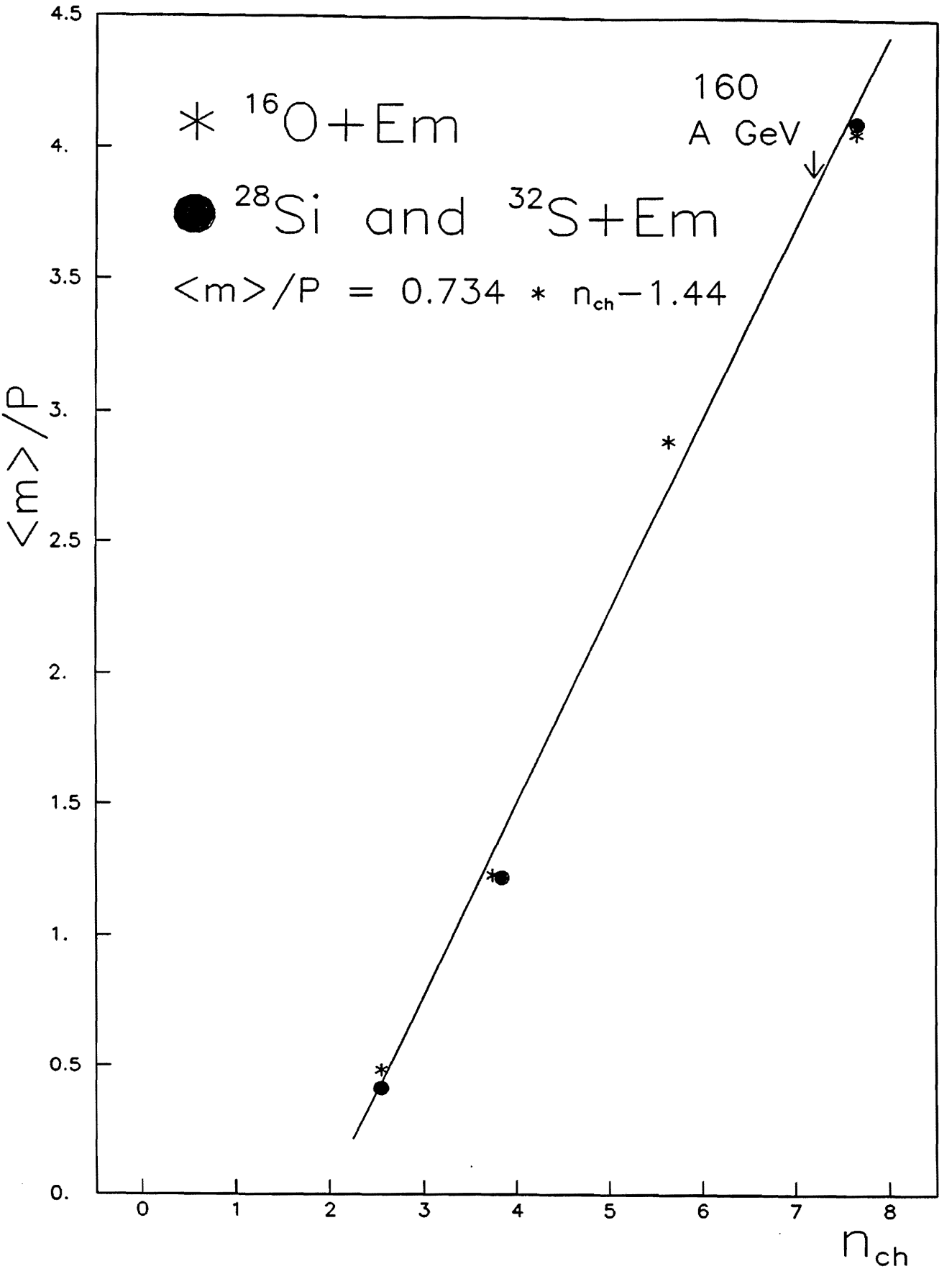
* ^{16}O+Em
^{28}Si and ^{32}S+Em
<m>/P = 0.734 * n_{ch}−1.44
160
A GeV
<m>/P
n_{ch}
0.
0.5
1.
1.5
2.
2.5
3.
3.5
4.
4.5
0
1
2
3
4
5
6
7
8

Fig. 9

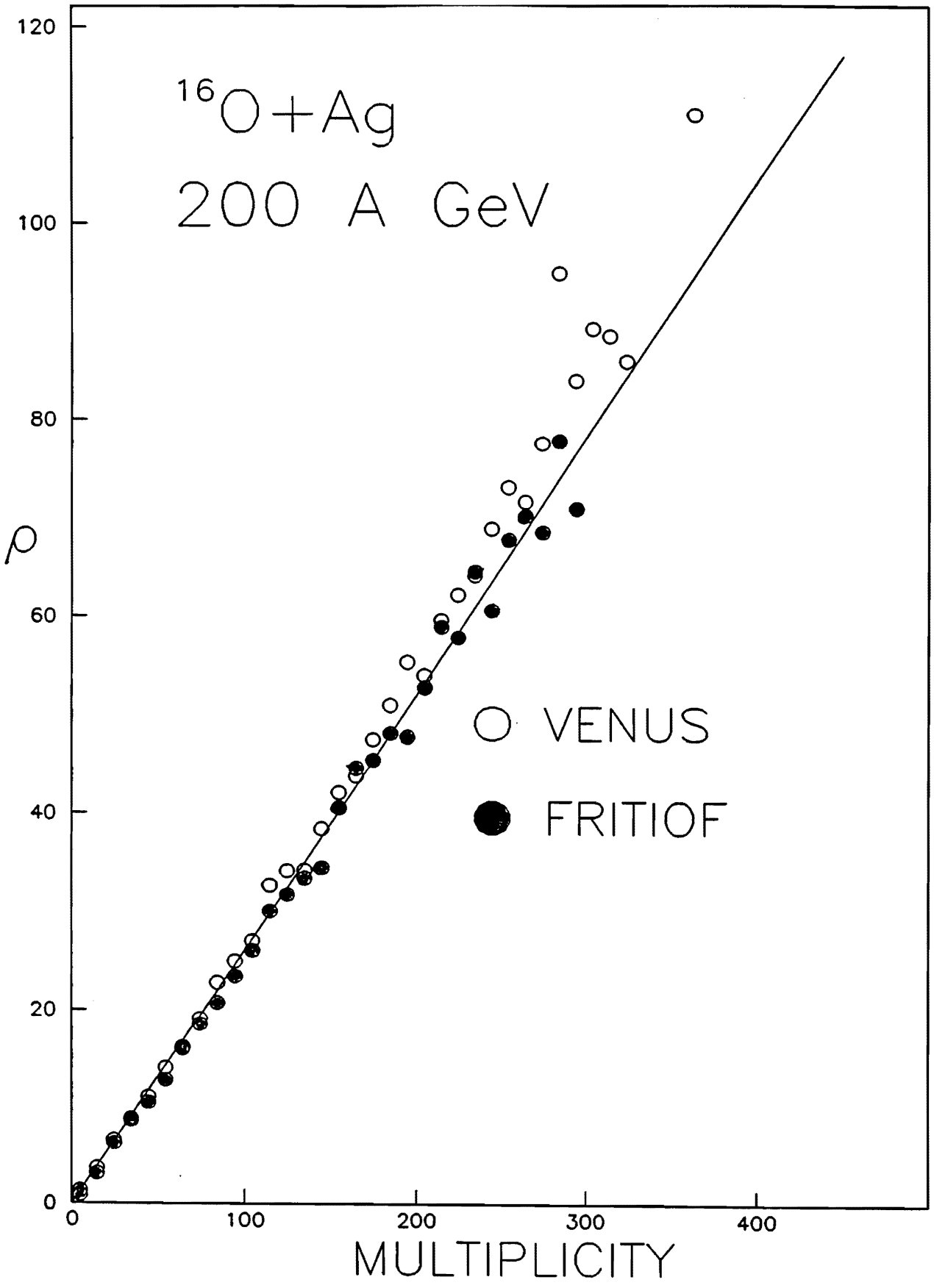
$^{16}O+Ag$
200 A GeV
VENUS
FRITIOF
ρ
MULTIPLICITY
0
20
40
60
80
100
120
0
100
200
300
400

Fig. 10

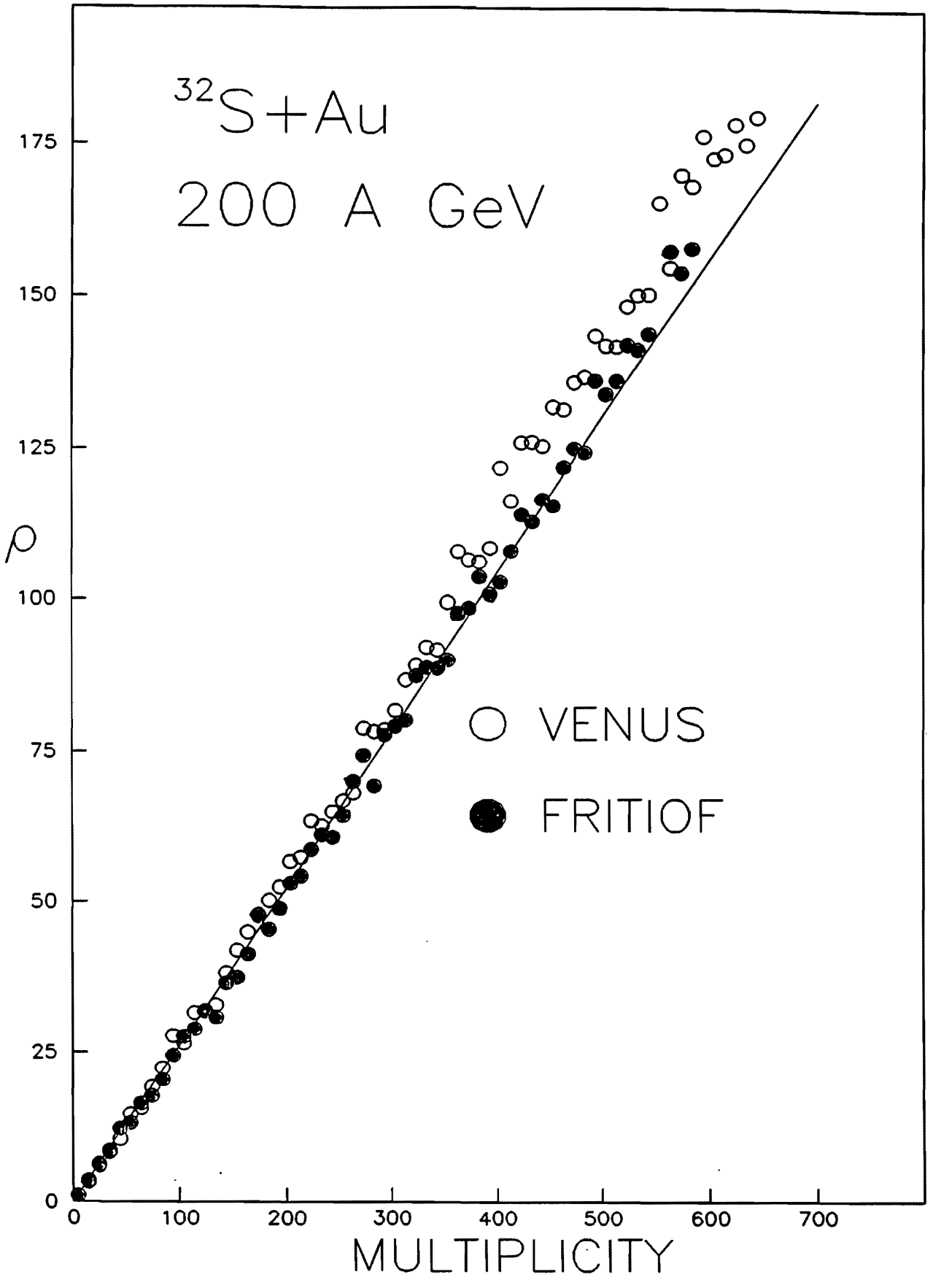
^{32}S+Au
200 A GeV
VENUS
FRITIOF
ρ
MULTIPLICITY
0
25
50
75
100
125
150
175
0
100
200
300
400
500
600
700

Fig. 11

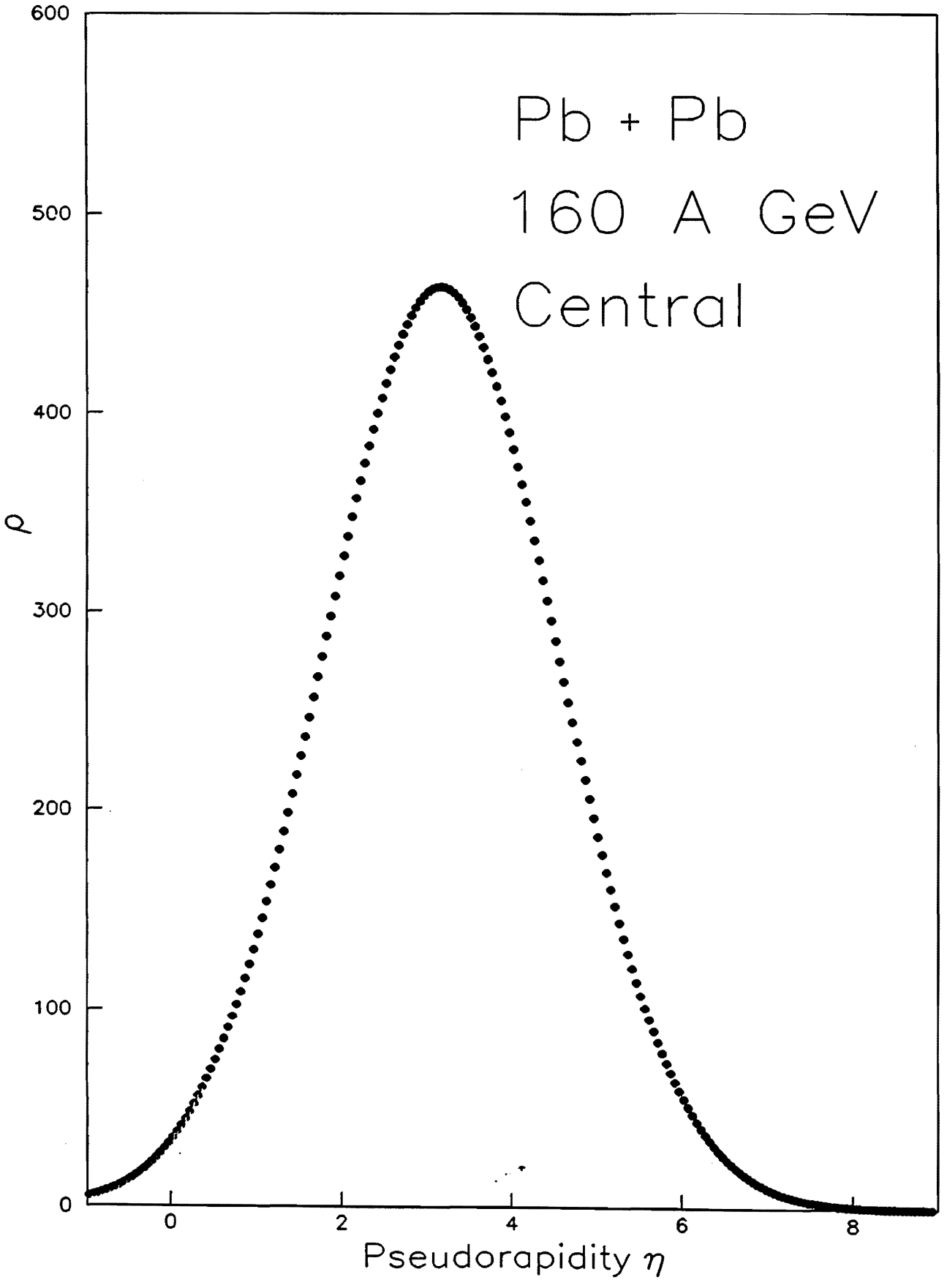
Pb + Pb
160 A GeV
Central
600
500
400
300
200
100
0
ρ
0
2
4
6
8
Pseudorapidity η

Fig. 12

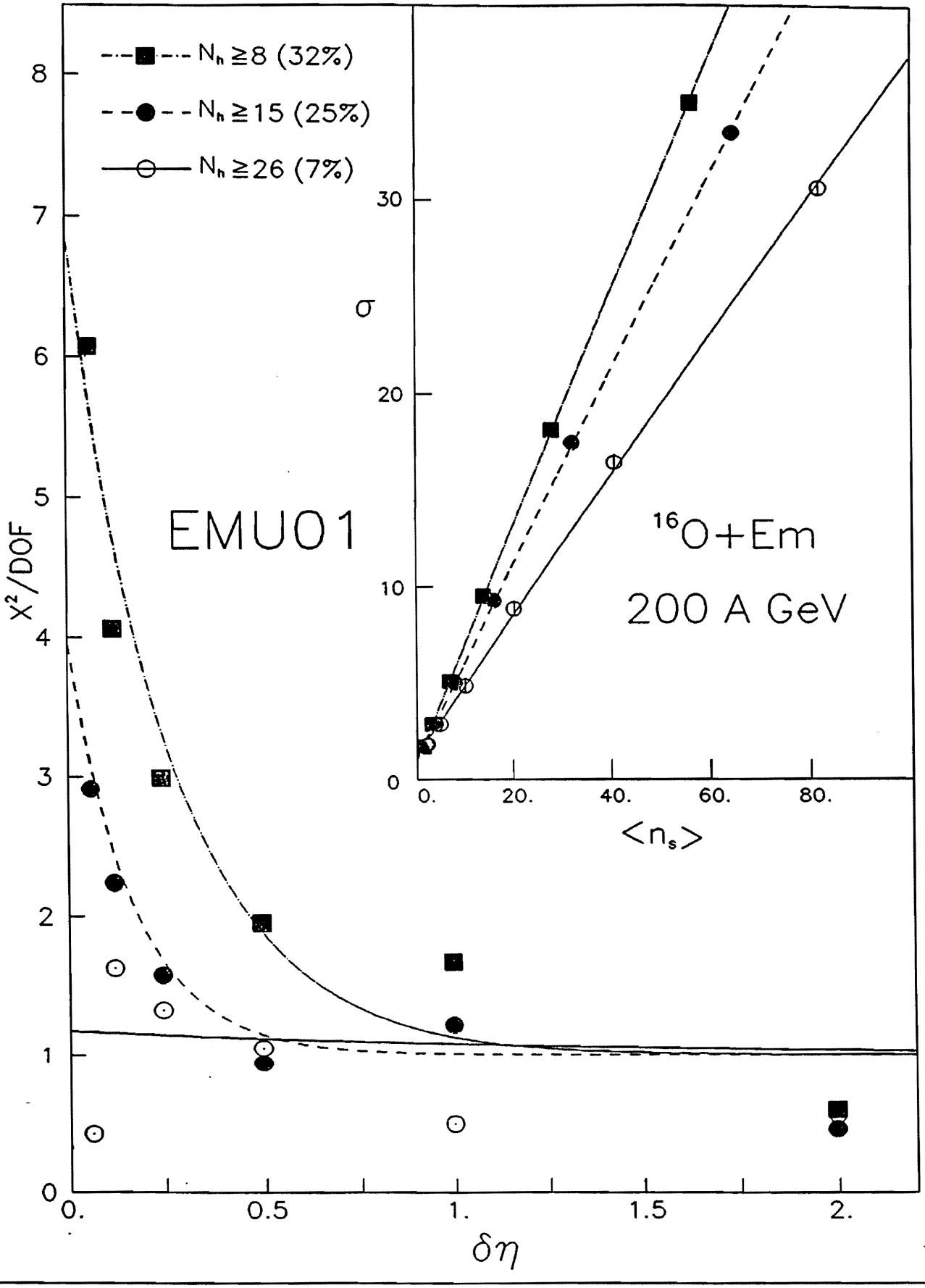
$N_h \geq 8$ (32%)
$N_h \geq 15$ (25%)
$N_h \geq 26$ (7%)
EMU01
$^{16}O+Em$
200 A GeV
X^2/DOF
$\delta\eta$
σ
$\langle n_s \rangle$

Fig. 13

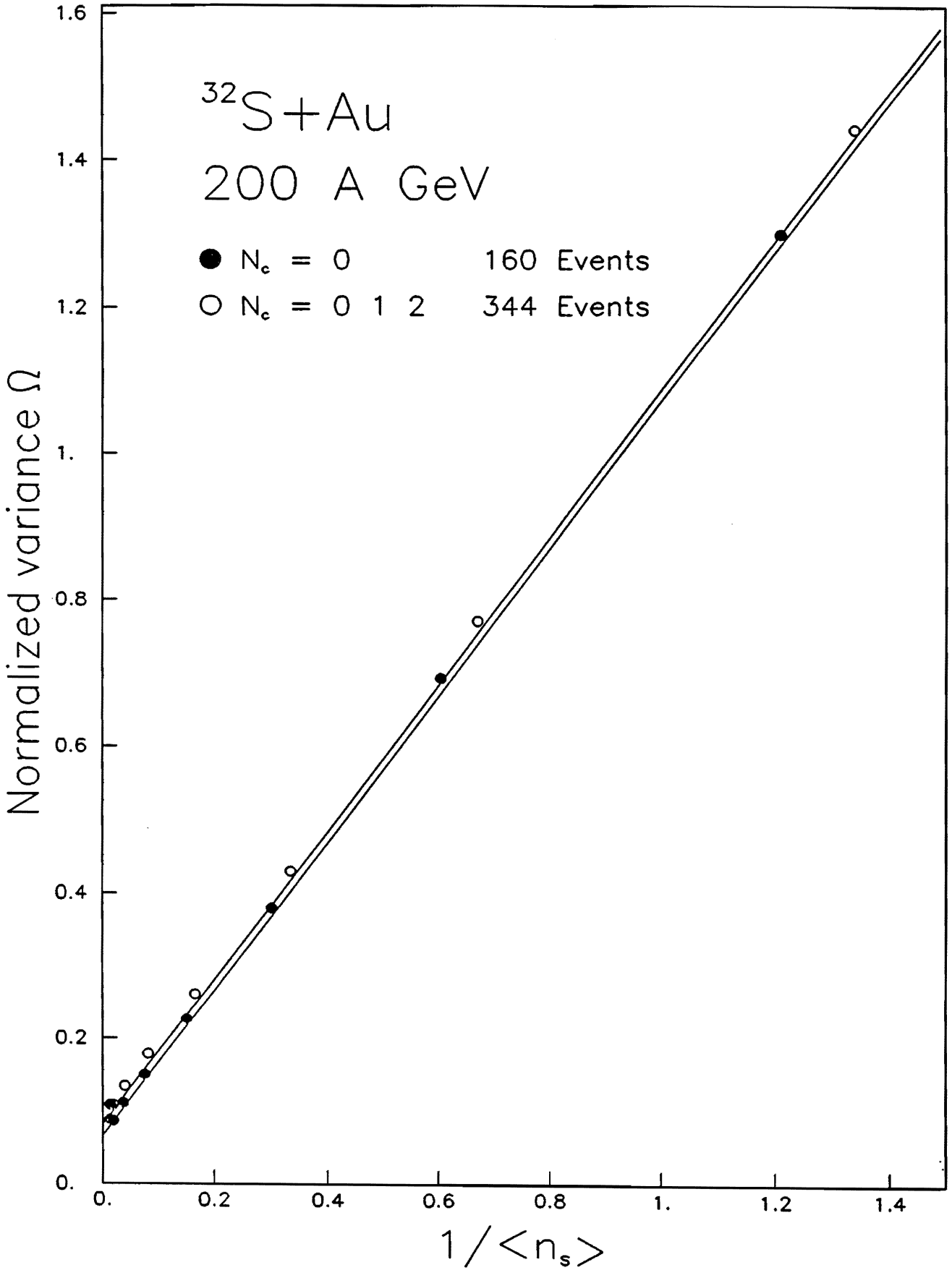
$^{32}S+Au$
200 A GeV
● N_c = 0 160 Events
○ N_c = 0 1 2 344 Events
Normalized variance Ω
1/<n_s>
0.
0.2
0.4
0.6
0.8
1.
1.2
1.4
1.6

Fig. 14

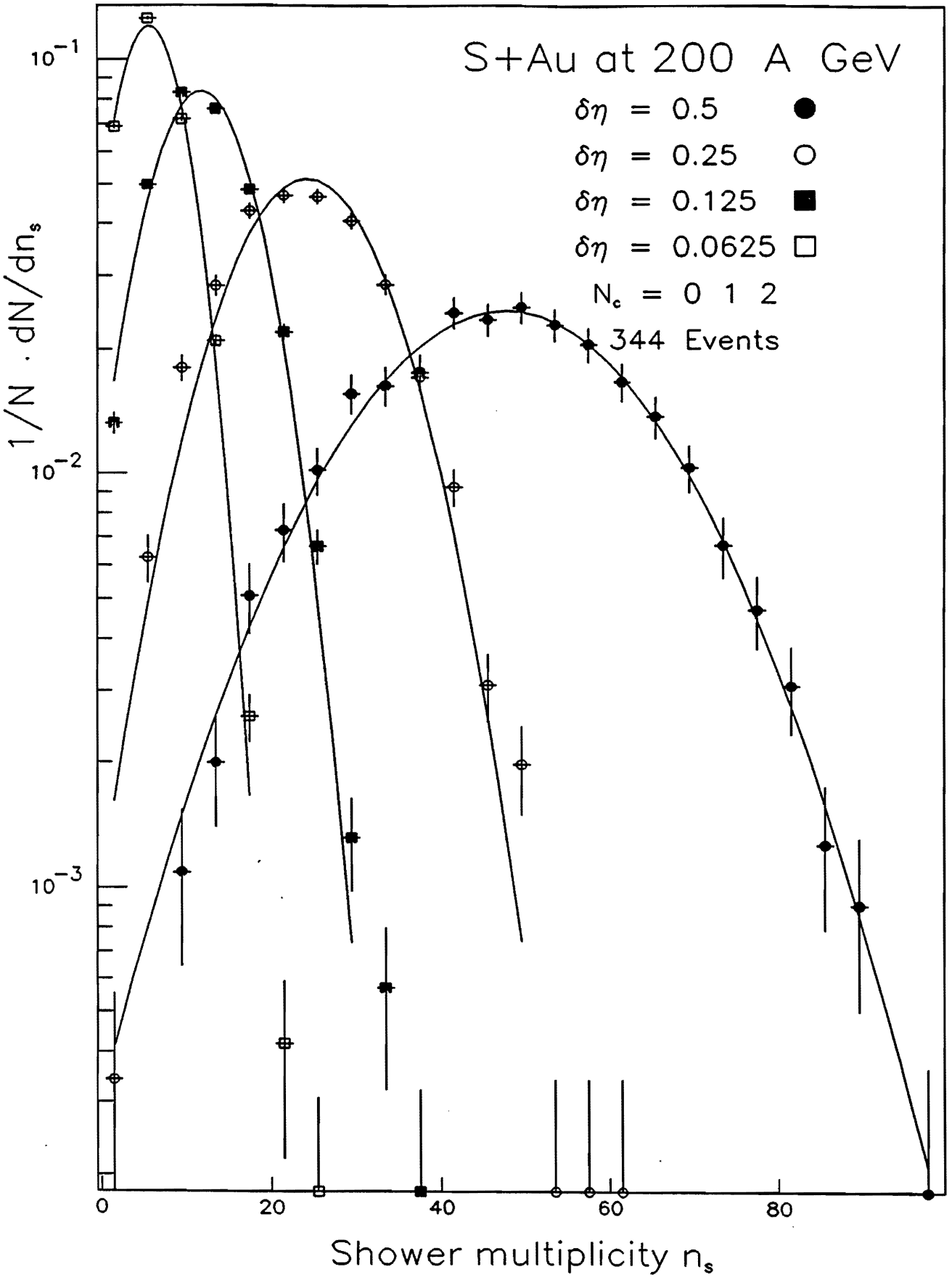
S+Au at 200 A GeV
δη = 0.5
δη = 0.25
δη = 0.125
δη = 0.0625
N_c = 0 1 2
344 Events
1/N · dN/dn_s
10^-1
10^-2
10^-3
0
20
40
60
80
Shower multiplicity n_s

Fig. 15

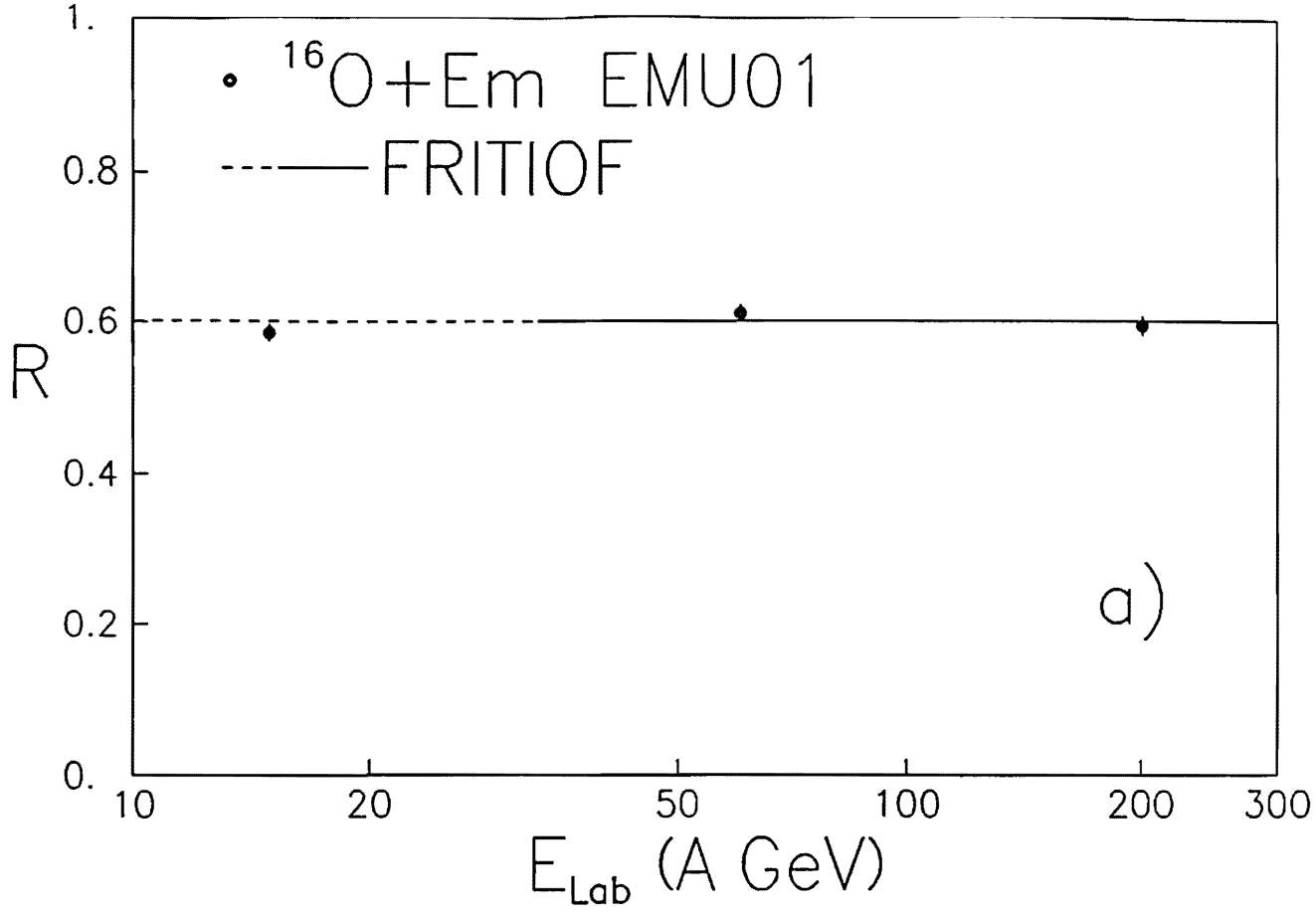
1.
0.8
0.6
0.4
0.2
0.
R
^{16}O+Em EMU01
FRITIOF
a)
10
20
50
100
200
300
E_{Lab} (A GeV)

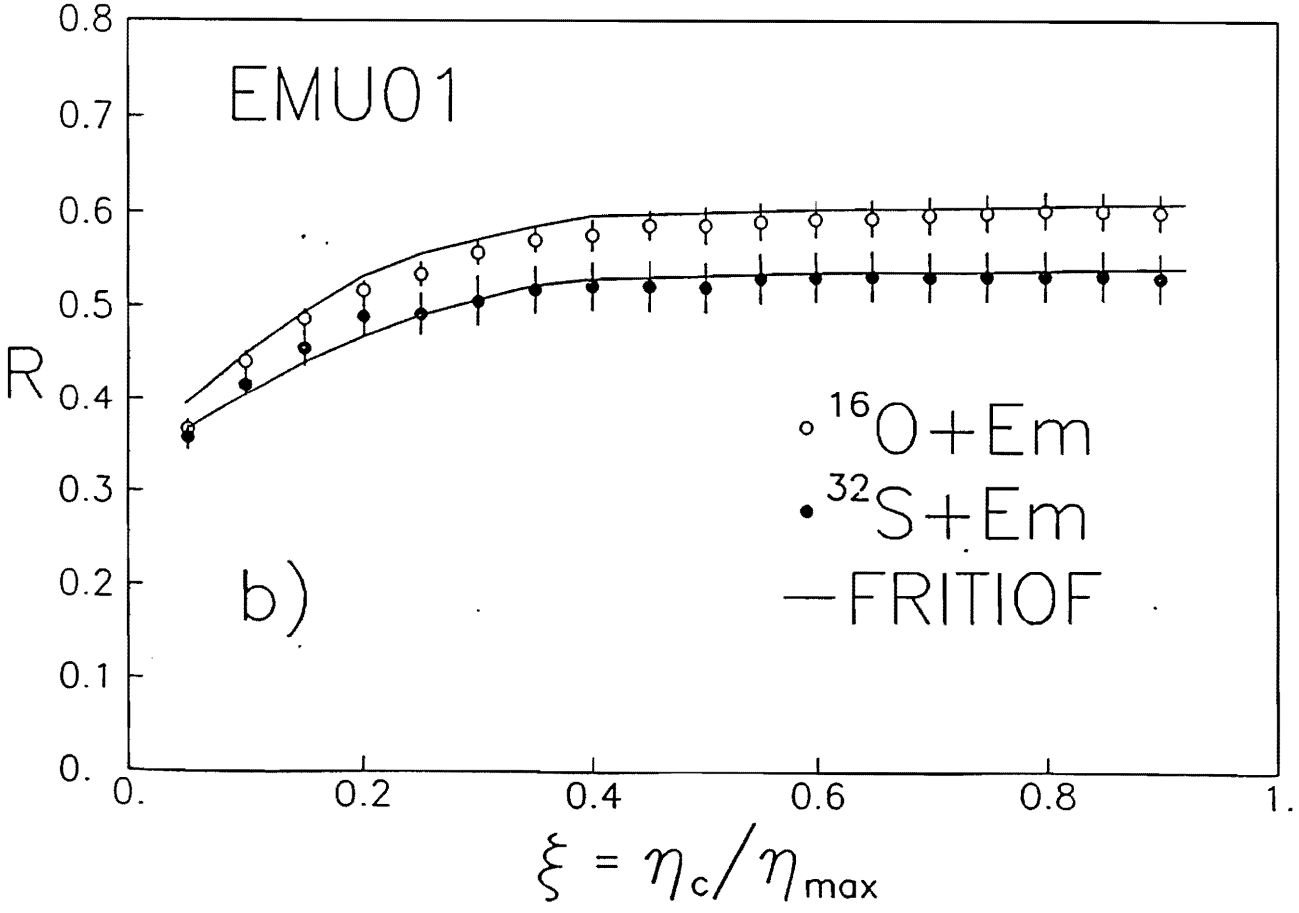
0.8
0.7
0.6
0.5
0.4
0.3
0.2
0.1
0.
R
EMU01
^{16}O+Em
^{32}S+Em
FRITIOF
b)
0.
0.2
0.4
0.6
0.8
1.
$\xi = \eta_c/\eta_{max}$